Available online at www.sciencedirect.com
SCIENCE DIRECT®
Journal of Sound and Vibration 293 (2006) 16–37
JOURNAL OF SOUND AND VIBRATION
www.elsevier.com/locate/jsvi

Identification of weak nonlinearities on damping and stiffness by the continuous wavelet transform

Minh-Nghi Ta*, Joseph Lardiès

Laboratoire de Mécanique Appliquée R. Chaléat, Université de Franche-Comté, FEMTO-ST, UMR CNRS 6174, 24 rue de l'Epitaphe 25000 Besançon, France

Received 23 June 2004; received in revised form 14 July 2005; accepted 20 September 2005
Available online 18 November 2005

Abstract

We consider the free response of a nonlinear vibrating system. Using the ridges and skeletons of the continuous wavelet transform, we identify weak nonlinearities on damping and stiffness and estimate their physical parameters. The crucial choice of the son wavelet function is obtained using an optimization technique based on the entropy of the continuous wavelet transform. The method is applied to simulated single-degree-of-freedom systems and multi-degree-of-freedom systems with nonlinearities on damping and stiffness. Experimental validation of the nonlinear identification and parameter estimation method is presented. The experimental system is a clamped beam with nonlinearities on damping and stiffness and these nonlinearities are identified and quantified from a displacement sensor.

1. Introduction

The identification and estimation of nonlinear parameters in vibrating systems is very important when models for the prediction of systems performance are developed. A number of techniques for nonlinear system identification have been developed. These techniques can be divided into two categories according to the choice of model form. The first category, mainly used in control engineering, deals with the first-order state space equation. The second category, mainly used in mechanical engineering, deals with the second-order equations of motion derived from Newton laws. In this paper we consider the second category. A number of procedures have been proposed for the identification of nonlinearities in vibrating systems. Of these, the application of the Hilbert transform to the impulse response of the system provides information about instantaneous amplitude and phase of the signal. Relationships between the instantaneous amplitude and frequency and between instantaneous amplitude and damping are constructed. Backbone and damping curves are then plotted by Feldman [1]. The Hilbert transform gives effective results for single-degree-of-freedom (sdof) systems. Applications to multi-degree-of-freedom (mdof) systems have proved difficult since the

*Corresponding author.
E-mail addresses: minh_nghi.ta@edu.univ-fcomte.fr (M.-N. Ta), joseph.lardies@univ-fcomte.fr (J. Lardiès).

0022-460X/$ - see front matter © 2005 Elsevier Ltd. All rights reserved.
doi:10.1016/j.jsv.2005.09.021

analysis requires band-pass filtration of the signal, in order to pick out each mode of interest and to reject all the others. This can produce bad results for systems with close modes. An improvement can be achieved if the wavelet transform is used instead of the Hilbert transform. A non-parametric identification technique is presented by Masri and Caughey [2]. They use information about state variables of nonlinear systems to express the system characteristics in terms of orthogonal functions. The method can be used with deterministic or random excitation to identify arbitrary nonlinearities. However, the method requires information regarding the displacement, velocity, acceleration and restoring forces acting on the system to determine by regression techniques nonlinearities. A great effort has to be spent in processing the data. A spectral method for identifying nonlinear structures has been proposed by Shyu [3]. This method uses a multichannel autoregressive time-series model to calculate the higher-order coherence function which is used to identify the order of nonlinearity. The method uses short record length and is very useful if the signals are transient or only short data length is available. However, the proposed procedure dealt only with the qualification or identification of the type of nonlinearities. The quantification of nonlinearities is not studied. The extended Kalman filter is an adaptation of the discrete Kalman filter and is used by Yun and Shinozuka [4] to determine nonlinearities. The extended Kalman filter is obtained by linearizing the nonlinear model into a Taylor series expansion. Yun and Shinozuka add a smoothing filter to improve results. Yang and Lin [5] present an on-line adaptive tracking technique, based on the recursive least-squares estimation, to identify the system parameters and their changes of nonlinear hysteretic structures. The tracking algorithm is based on the adaptation of the current measured data to determine the parameter variations, so that the residual error is contributed only by noises. The method uses displacement, velocity and acceleration to determine a recursive solution of system parameters. Simulation results, using sdof and 2dof, for nonlinear hysteretic structures are presented in the paper [5].

The continuous wavelet transform is a method that converts a time response representation in 1D space into a time–frequency response in 2D space. The continuous wavelet transform technique has the advantage that it requires to measure only the displacement or velocity or acceleration of the system. It is not necessary to know displacement and velocity and acceleration simultaneously as in the case of non-parametric identification methods. The continuous wavelet transform has been used successfully to obtain natural frequencies and damping ratios of linear vibrating systems. Numerical and experimental results are presented in Refs. [6–10]. Identification of nonlinear systems using the continuous wavelet transform has been studied by Staszewski [11], Argoul and Le [12], Garibaldi et al. [13] and Lenaerts et al. [14]. Staszewski [11] uses the Morlet wavelet as analysing function and presents two simulated examples. The first example analyses a sdof system with Coulomb friction and cubic stiffness nonlinearities. The second example analyses a 2dof system with cubic stiffness nonlinearities. These nonlinearities are identified but not quantified. In Ref. [12], Argoul and Le consider the Cauchy wavelet as analysing function and use accelerometer responses of a clamped beam. With limitation to the first mode, they represent the beam by an oscillator with a cubic nonlinearity and a weak viscous damping. In Ref. [13] Garibaldi et al. identify only nonlinear damping mechanisms using the continuous wavelet transform. In Ref. [14] Lenaerts et al. identify a nonlinear system using two different method: a method based on the continuous wavelet transform and a method using the restoring force surface. Both techniques exploit the system free response and results in the estimation of linear and nonlinear physical parameters are giving using experimental data.

In this paper we use the continuous wavelet transform to identify and quantify weak nonlinearities of vibrating systems. Numerical and experimental results using a clamped beam with different classes of nonlinearities on damping and stiffness are presented.

This paper is organized as follows. In Section 2 the approximate equations of amplitude and phase are derived for a sdof system with nonlinearities on damping and stiffness. In Section 3 the continuous wavelet transform and its properties are introduced. A wavelet entropy technique is used to determine the optimal value of a parameter used with the analysing wavelet function. The main concept of continuous wavelet transform ridges, skeletons and free response recovery procedures are also described. In Section 4 we apply the method to simulated sdof and mdof systems with nonlinearities on damping and stiffness. Experimental validation of the method is presented using a clamped beam with nonlinearities on damping and stiffness. This paper is briefly concluded in Section 5.

2. Response of a nonlinear sdof system

2.1. General case

Consider the general differential equation governing the free vibration of systems having a sdof

$$\ddot{x} + \omega_n^2 x + \varepsilon f(x, \dot{x}) = 0, \tag{1}$$

where ω_n is the natural angular frequency of the linear system, ε is a small dimensionless parameter and $f(x, \dot{x})$ a general nonlinear function of displacement x and velocity $\dot{x}$. The dot indicates time derivative, as usual. It is well known that for the corresponding linear problem ($\varepsilon = 0$) the solution is $x(t) = A\cos(\omega_n t + \beta)$ where A and β are constants. For the determination of the analytical solution of Eq. (1) we use the method of Krylov–Bogoliubov [15–17], called also the averaging method. Using this method a solution to a nonlinear equation (1) can be sought in the form

$$x(t) = A(t)\cos(\omega_n t + \beta(t)) = A(t)\cos(\varphi(t)), \tag{2}$$

where $\varphi(t) = \omega_n t + \beta(t)$; $A(t)$ and $\varphi(t)$ are the amplitude and phase modulation of the system free response which are time-dependent functions. However, this procedure introduces an excessive variability into the solution; consequently, an additional restriction may be introduced: it is convenient to require the velocity $\dot{x}(t)$ to have the same form as the harmonic oscillator. We obtain then:

$$\dot{A}(t)\cos(\varphi(t)) - A(t)\dot{\beta}(t)\sin(\varphi(t)) = 0. \tag{3}$$

The second derivative of the assumed solution is now formed and these relations are introduced into the differential equation (1) to obtain

$$\omega_n \dot{A}(t)\sin(\varphi(t)) + \omega_n A(t)\dot{\beta}(t)\cos(\varphi(t)) = \varepsilon f(A(t)\cos(\varphi(t)), -\omega_n A(t)\sin(\varphi(t))). \tag{4}$$

Solving Eqs. (3) and (4) for $\dot{A}(t)$ and $\dot{\beta}(t)$ we obtain

$$\dot{A}(t) = \frac{\varepsilon}{\omega_n}\sin(\varphi(t)) f(A(t)\cos(\varphi(t)), -\omega_n A(t)\sin(\varphi(t))), \tag{5}$$

$$\dot{\beta}(t) = \frac{\varepsilon}{\omega_n A(t)}\cos(\varphi(t)) f(A(t)\cos(\varphi(t)), -\omega_n A(t)\sin(\varphi(t))). \tag{6}$$

The second-order nonlinear differential equation (1) has been transformed into two first-order differential equations for $A(t)$ and $\beta(t)$. The expression for $\dot{A}(t)$ and $\dot{\beta}(t)$ may now be expanded in Fourier series

$$\dot{A}(t) = \frac{\varepsilon}{\omega_n}\left\{K_0(A) + \sum_{n=1}^{r}[K_n(A)\cos(n\varphi(t)) + L_n(A)\sin(n\varphi(t))]\right\}, \tag{7}$$

$$\dot{\beta}(t) = \left(\frac{\varepsilon}{\omega_n A(t)}\right)\left\{P_0(A) + \sum_{n=1}^{r}[P_n(A)\cos(n\varphi(t)) + Q_n(A)\sin(n\varphi(t))]\right\}, \tag{8}$$

where

$$K_0(A) = \frac{1}{2\pi}\int_0^{2\pi}\sin(\varphi(t)) f(A(t)\cos(\varphi(t)), -\omega_n A(t)\sin(\varphi(t)))\,\mathrm{d}\varphi, \tag{9}$$

$$P_0(A) = \frac{1}{2\pi}\int_0^{2\pi}\cos(\varphi(t)) f(A(t)\cos(\varphi(t)), -\omega_n A(t)\sin(\varphi(t)))\,\mathrm{d}\varphi. \tag{10}$$

During one cycle, the variation of $\dot{A}(t)$ and $\dot{\beta}(t)$ is small because of the presence of the small parameter ε in Eqs. (7) and (8). Hence, the average values of $\dot{A}(t)$ and $\dot{\beta}(t)$ are considered. Since the motion is over a single cycle, and since the terms under the summation signs are of the same period and consequently vanish, we

obtain approximately:

$$\dot{A}(t) = \frac{\varepsilon}{\omega_n} K_0(A) = \frac{\varepsilon}{2\pi\omega_n} \int_0^{2\pi} \sin(\varphi(t)) f(A(t)\cos(\varphi(t)), -\omega_n A(t)\sin(\varphi(t))) \, \mathrm{d}\varphi, \tag{11}$$

$$\dot{\beta}(t) = \left(\frac{\varepsilon}{\omega_n A(t)}\right) P_0(A) = \left(\frac{\varepsilon}{2\pi\omega_n A(t)}\right) \int_0^{2\pi} \cos(\varphi(t)) f(A(t)\cos(\varphi(t)), -\omega_n A(t)\sin(\varphi(t))) \, \mathrm{d}\varphi. \tag{12}$$

These two equations allow to easily obtain an approximate analytical solution describing the free behaviour of a sdof system, for different forms of the nonlinear function $f(x, \dot{x})$.

2.2. Envelope and phase of a nonlinear damping system

By application of the above procedure consider a composite damping system which is defined by

$$\varepsilon f(\dot{x}) = \sum_{i=0}^{p} \mu_i |\dot{x}|^i \operatorname{sgn}(\dot{x}), \tag{13}$$

where p is the order considered in the damping system and μ_i is the ith damping coefficient normalized to the mass. The approximate free response of a sdof system with a composite damping can be obtained using Eqs. (11) and (12)

$$\begin{aligned} \dot{A}(t) &= -\frac{1}{\pi\omega_n} \int_0^{\pi} \sum_{i=0}^{p} \mu_i \omega_n^i A^i(t) \sin^{i+1}\varphi \, \mathrm{d}\varphi \\ &= -\sum_{i=0}^{p} \frac{1}{\sqrt{\pi}} \mu_i \omega_n^{i-1} \frac{\Gamma(i/2+1)}{\Gamma(i/2+3/2)} A^i(t) = \sum_{i=0}^{p} c_i A^i(t), \end{aligned} \tag{14}$$

where Γ is the function gamma [16] and

$$c_i = -\frac{1}{\sqrt{\pi}} \mu_i \omega_n^{i-1} \frac{\Gamma(i/2+1)}{\Gamma(i/2+3/2)}, \tag{15}$$

$$\dot{\beta}(t) = \frac{1}{2\pi\omega_n A(t)} \int_0^{2\pi} \sum_{i=0}^{p} \mu_i |-\omega_n A(t)\sin(\varphi(t))|^i \operatorname{sgn}(-\omega_n A(t)\sin(\varphi(t))) \cos\varphi \, \mathrm{d}\varphi = 0. \tag{16}$$

This value implies that for a composite damping mechanism the phase angle $\beta(t)$ does not change over time: $\beta(t) = \beta_0$ which is constant. It is important to note that nonlinearities on damping have only an impact on the envelope $A(t)$ and they do not affect the phase $\beta(t)$ which remains constant.

Our objective is to determine $A(t)$, $\dot{A}(t)$ and use Eq. (14) for the identification of the order p and the estimation of coefficients c_i. The envelope $A(t)$ will be determined from the ridges of the continuous wavelet transform presented in the next section. From the couple (p, c_i), it is easy to identify the composite damping mechanism and to quantify the damping coefficients μ_i from Eq. (15). For example, if we have a second-order composite damping system ($p = 2$) with Coulomb damping (μ_0), linear damping (μ_1) and square damping (μ_2), we obtain: $\dot{A}(t) = c_0 + c_1 A(t) + c_2 A^2(t)$ with the coefficients

$$c_0 = -\frac{2\mu_0}{\pi\omega_n}; \quad c_1 = -\frac{\mu_1}{2}; \quad c_2 = -\frac{4\omega_n\mu_2}{3\pi}.$$

2.3. Envelope and phase of a nonlinear damping and nonlinear stiffness system

Consider a sdof system with nonlinearities on damping and stiffness of the form

$$\varepsilon f(\dot{x}, x) = \sum_{i=0}^{p} \mu_i |\dot{x}|^i \operatorname{sgn}(\dot{x}) + \eta_q |x|^q \operatorname{sgn}(x), \tag{17}$$

where η_q is the qth order mass normalized nonlinear stiffness. The expression for $\dot{A}(t)$ is the sum of two terms: the term due to nonlinear damping and the term due to nonlinear stiffness. Using Eq. (11) we obtain

$$\dot{A}(t) = \dot{A}_1(t) + \dot{A}_2(t) \tag{18}$$

with

$$\begin{aligned}\dot{A}(t) &= -\frac{1}{\pi\omega_n}\int_0^{\pi}\sum_{i=0}^{p}\mu_i\omega_n^i A^i(t)\sin^{i+1}\varphi\,\mathrm{d}\varphi \\ &= -\sum_{i=0}^{p}\frac{1}{\sqrt{\pi}}\mu_i\omega_n^{i-1}\frac{\Gamma(i/2+1)}{\Gamma(i/2+3/2)}A^i(t) = \sum_{i=0}^{p}c_i A^i(t),\end{aligned} \tag{19}$$

$$\dot{A}_2(t) = \frac{\eta_q}{2\pi\omega_n}\int_0^{2\pi}\sin(\varphi(t))|A(t)\cos(\varphi(t))|^q\,\mathrm{sgn}(A(t)\cos(\varphi(t)))\,\mathrm{d}\varphi = 0. \tag{20}$$

It is important to note that nonlinearities on stiffness does not affect the amplitude decay of the signal; only nonlinearities on damping affect the envelope of the signal. The expression for $\dot{\beta}(t)$ is again the sum of two terms: the term due to nonlinear damping and the term due to nonlinear stiffness. Using Eq. (12) we obtain

$$\dot{\beta}(t) = \dot{\beta}_1(t) + \dot{\beta}_2(t) \tag{21}$$

with

$$\dot{\beta}_1(t) = \frac{1}{2\pi\omega_n A(t)}\int_0^{2\pi}\sum_{i=0}^{p}\mu_i|-\omega_n A(t)\sin(\varphi(t))|^i\,\mathrm{sgn}(-\omega_n A(t)\sin(\varphi(t)))\cos\varphi\,\mathrm{d}\varphi = 0, \tag{22}$$

$$\begin{aligned}\dot{\beta}_2(t) &= \frac{\eta_q}{2\pi\omega_n A(t)}\int_0^{2\pi}|A(t)\cos(\varphi(t))|^q\,\mathrm{sgn}(A(t)\cos(\varphi(t)))\cos\varphi\,\mathrm{d}\varphi, \\ \dot{\beta}_2(t) &= \frac{\eta_q A^{q-1}(t)}{2\omega_n}[1+(-1)^{q+1}]\left[\frac{\Gamma(q+2)}{2^{q+1}(\Gamma(q/2+3/2))^2}\right] = r_q A^{q-1}(t),\end{aligned} \tag{23}$$

where

$$r_q = \frac{\eta_q}{2\omega_n}[1+(-1)^{q+1}]\left[\frac{\Gamma(q+2)}{2^{q+1}(\Gamma(q/2+3/2))^2}\right]. \tag{24}$$

It is important to note that nonlinearities on damping do not affect the phase of the signal. Only nonlinearities on stiffness have an influence on the phase $\beta(t)$ of the signal. Our objective is to determine $\dot{\beta}(t)$ and use Eqs. (23) and (24) for the identification of the order q and quantification of nonlinearities on stiffness from r_q. For example if we consider a Duffing oscillator where a cubic stiffness is used ($q = 3$) we have $r_3 = 3\eta_3/8\omega_n$. The phase $\beta(t)$ will be determined from the ridges of the continuous wavelet transform presented in the next section.

3. The continuous wavelet transform

3.1. Definitions and theoretical background

The Fourier transform of a function (or a signal) $x(t)$ is a linear transformation based on the decomposition of this function in terms of a basis of elementary functions $\mathrm{e}^{-\mathrm{j}\omega t}$ and is given by

$$\mathrm{TF}[x] = \hat{x}(\omega) = \int_{-\infty}^{+\infty}x(t)\mathrm{e}^{-\mathrm{j}\omega t}\,\mathrm{d}t. \tag{25}$$

This decomposition does not give any local time information about the function $x(t)$. A localized decomposition can be obtained using the continuous wavelet transform. Under assumptions that all functions

$x(t)$ satisfy the condition

$$\int_{-\infty}^{+\infty} |x(t)|^2 \, \mathrm{d}t < \infty \tag{26}$$

which implies that $x(t)$ decays to zero at $\pm\infty$, as in the case of Fourier analysis, the idea of the continuous wavelet transform is to find a function $\psi(t)$ which can generate a basis for the entire space of functions $x(t)$. If the decay of this function is very fast, this function is called a small wave or a wavelet. The fast decay introduces locality into the analysis, which is not the case of the Fourier transform where a global representation is obtained. Using a family of basis functions, wavelets can be formulated to describe $x(t)$ in a localized time and frequency format. The continuous wavelet transform gives time and frequency information about the analysed data. The continuous wavelet transform of the function $x(t)$ is defined as [18,19]

$$W_\psi[x](a,b) = \langle x, \psi_{a,b} \rangle = \frac{1}{\sqrt{a}} \int_{-\infty}^{+\infty} x(t) \psi^* \left(\frac{t-b}{a} \right) \mathrm{d}t, \tag{27}$$

where $\psi(t)$ is the analysing or mother wavelet and $\psi^*(t)$ the complex conjugate of $\psi(t)$; b is the parameter localizing the wavelet function in the time domain: $W_\psi[x](a,b)$ shows the local information about $x(t)$ at the time $t = b$ and a is the dilatation or scale parameter defining the analysing window stretching. The idea of the continuous wavelet transform is to decompose a function $x(t)$ into wavelet coefficients $W_\psi[x](a,b)$ using the basis of wavelet functions. The wavelet coefficients represent a measure of the similitude between the dilated and shifted wavelet and the function $x(t)$ at time b and scale a. Any function $\psi(t)$ can be used as an analysing wavelet if it satisfies the admissibility condition [18–20]

$$c_\psi = \int_{-\infty}^{+\infty} \frac{|\hat{\psi}(\omega)|^2}{|\omega|} \, \mathrm{d}\omega < +\infty, \tag{28}$$

where $\hat{\psi}(\omega)$ is the Fourier transform of $\psi(t)$. It follows that $\hat{\psi}(\omega)$ is a continuous function, so that the finiteness of c_ψ implies that $\hat{\psi}(0) = 0$, or also that the mean value of $\psi(t)$ in the time domain is zero: $\int_{-\infty}^{+\infty} \psi(t) \, \mathrm{d}t = 0$. The admissibility condition is necessary to obtain the inverse of the wavelet transform [18,19]. The wavelet $\psi(t)$ must be also a window function to enable the possibility of time–frequency localization: $\psi(t)$ decays at infinity, which means that additionally

$$\int_{-\infty}^{+\infty} |\psi(t)| \, \mathrm{d}t < \infty. \tag{29}$$

If one assumes that $\psi(t)$ is a rapidly decaying function in time domain, that is the values of $\psi(t)$ are negligible outside the interval $(t_{\min}, t_{\max})$, the transform becomes local.

We can see the frequency localization when the continuous wavelet transform is expressed in terms of the Fourier transform. Using the Parseval identity [18–20], we can define the frequency domain formulation of the continuous wavelet transform

$$W_\psi[x](a,b) = \frac{\sqrt{a}}{2\pi} \int_{-\infty}^{+\infty} \hat{x}(\omega) \hat{\psi}^*(a\omega) \mathrm{e}^{\mathrm{j}\omega b} \, \mathrm{d}\omega. \tag{30}$$

This localization depends on the dilatation or scale parameter a.

A very useful property of the continuous wavelet transform is its linearity: the continuous wavelet transform of P signals is

$$W_\psi \left[\sum_{i=1}^{P} x_i \right] (a,b) = \sum_{i=1}^{P} W_\psi[x_i](a,b). \tag{31}$$

This property is very convenient for the analysis of multi-component signals: it is possible to analyse each component x_i of a multi-component signal.

A number of different analysing functions have been used in the wavelet analysis. One of the most known and widely used is the Morlet wavelet defined in the time domain as

$$\psi(t) = \mathrm{e}^{-t^2/2} \mathrm{e}^{\mathrm{j}\omega_0 t}, \tag{32}$$

where ω_0 is the wavelet frequency. The dilated version of the Fourier transform is

$$\hat{\psi}(a\omega) = \sqrt{2\pi}\mathrm{e}^{-1/2(a\omega-\omega_0)^2}. \tag{33}$$

In practice the value of ω_0 is chosen $\omega_0 \geqslant 5$ which meets approximately the requirements given by condition (28). Note that $\hat{\psi}(a\omega)$ is maximum at the central frequency $\omega_c = \omega_0/a$ and the Morlet wavelet can be viewed as a linear band-pass filter whose bandwidth is proportional to $1/a$ or to the central frequency. Thus, the value of the dilatation parameter a at which the wavelet filter is focused on the wavelet frequency can be determined from $a = \omega_0/\omega_c$.

In summary, the continuous wavelet transform analyses an arbitrary function $x(t)$ only locally at windows defined by a wavelet function. The continuous wavelet transform decomposes $x(t)$ into various components at different time windows and frequency bands. The size of the time window is controlled by the translation parameter b while the length of the frequency band is controlled by the dilatation parameter a. Hence, one can examine the signal at different time windows and frequency bands by controlling translation and dilatation. However, constrained by the uncertainty principle [19], a compromise usually has to be made choosing either a narrow time window for good time resolution, or a wide time window for good frequency resolution. In order to control the shape of the analysing wavelet we introduce the modified Morlet wavelet.

3.2. The modified Morlet wavelet and the wavelet entropy

We consider the Morlet wavelet function and introduce a parameter N which controls the shape of the basic wavelet: this parameter balances the time resolution and the frequency resolution of the Morlet wavelet. The modified Morlet wavelet function used in this paper is

$$\psi(t) = \mathrm{e}^{-t^2/N}\mathrm{e}^{\mathrm{j}\omega_0 t} \tag{34}$$

with $N > 0$ and whose dilated version of its Fourier transform is

$$\hat{\psi}(a\omega) = \sqrt{N\pi}\mathrm{e}^{-N/4(a\omega-\omega_0)^2}. \tag{35}$$

An important value of N gives a narrower spectrum allowing a better frequency resolution, but at the expense of time resolution. So, there always exists an optimal N that has the best time–frequency resolution for a certain signal localized in the time–frequency plane. This modified Morlet wavelet function offers a better compromise in terms of localization, in both time and frequency for a signal, than the traditionally Morlet wavelet function. The optimal value of N is obtained by minimizing the entropy of the wavelet coefficients introduced here.

We assume that the signal $x(t)$ is given by sampled values $\{x(q)\}$, $q = 1, 2, \ldots, Q$. The total energy of this sequence is $\sum_q |x(q)|^2$ and the values

$$p(q) = \frac{|x(q)|^2}{\sum_q |x(q)|^2} \tag{36}$$

give the probability distribution of the signal's energy in the time domain. Furthermore, in the wavelet multiresolution analysis of the time series $\{x(q)\}$ the energy for each scale a_i is

$$E_{ai} = \sum_j |W_\psi[x](a_i, b_j)|^2. \tag{37}$$

E_{ai} is then obtained with a set of wavelet coefficients over a number of translations b_j, given a particular scale a_i. As a consequence, the total energy can be obtained by $E_{\text{total}} = \sum_i E_{ai}$. Then the normalized values, $p_{ai} = E_{ai}/E_{\text{total}}$, which represent the relative wavelet energy for $i = 1, 2, \ldots, M$ define by scale the probability distribution of the energy. Clearly, $\sum_i p_{ai} = 1$ and the distribution $\{p_{ai}\}$ can be considered as a time-scale density. The Shannon entropy [21,22] gives a useful criteria for analysing and comparing these distributions, since it provides a measure of the information of any distribution. Following the definition of entropy given by

Shannon, we define the time varying wavelet entropy as

$$WE = -\sum_i p_{ai} \log(p_{ai}) \tag{38}$$

which measures the degree of disorder or unpredictability of energy in each continuous wavelet transform. Using the modified Morlet wavelet there exists an optimal value of the parameter N obtained by minimization of the wavelet entropy. An example is presented in the next section verifying the validity of the wavelet entropy.

3.3. Ridge and skeleton of the continuous wavelet transform

Mallat [18] and Torresani [20] give the definition of a class of signals called asymptotic and present some results for the time–frequency analysis of such signals. A signal of form (2) is asymptotic if the amplitude $A(t)$ varies slowly compared to the variations of the phase $\varphi(t)$, or in a more rigorous way

$$\dot{\varphi}(t) = \omega_n + \dot{\beta}(t) > 0 \quad \text{and} \quad \left|\frac{1}{\dot{\varphi}(t)}\right|\left|\frac{\dot{A}(t)}{A(t)}\right| < \varepsilon, \tag{39}$$

where ε is a small real positive number. The analytic signal associated with the asymptotic signal is $x_a(t) = A(t)e^{j\varphi(t)}$ and from this definition, Mallat [18] proposed the concept of instantaneous angular frequency as the time varying derivative of the phase: $\omega(t) = \dot{\varphi}(t)$. The continuous wavelet transform of an asymptotic signal $x(t)$ is obtained by asymptotic techniques and is expressed as [18,20]

$$W_\psi[x](a,b) = \frac{\sqrt{a}}{2} A(b) e^{j\varphi(b)} \hat{\psi}^*(a\dot{\varphi}(b)). \tag{40}$$

Using the modified Morlet wavelet, we have

$$W_\psi[x](a,b) = \frac{\sqrt{a}}{2} \sqrt{N\pi} A(b) e^{-N/4(a\dot{\varphi}(b)-\omega_0)^2} e^{j\varphi(b)}. \tag{41}$$

The square of the modulus of the continuous wavelet transform can be interpreted as an energy density distribution over the time-scale plane. The energy of the signal is essentially concentrated on the time-scale plane around a region called the ridge of the continuous wavelet transform. In other words, the ridge of the continuous wavelet transform is the region containing the points defined by $a = a(b)$, where the amplitude of the continuous wavelet transform is maximum. The ridges are identified by seeking out the points where the continuous wavelet transform coefficients take on local maximum values: for each value of b, we obtain a value of a such as $|W_\psi[x](a(b),b)| = \max_a |W_\psi[x](a,b)|$. To obtain the ridge, the dilatation parameter $a = a(b)$ has to be calculated in order to maximize the analysing wavelet $\hat{\psi}^*(a\dot{\varphi}(b))$, that is using the modified Morlet wavelet, for $a = a(b) = \omega_0/\dot{\varphi}(b)$. The values of the continuous wavelet transform that are restricted to the ridge are the skeleton of the continuous wavelet transform. We obtain

$$W_\psi[x](a(b),b) = \frac{\sqrt{a(b)}}{2} \sqrt{N\pi} A(b) e^{j\varphi(b)}. \tag{42}$$

It is important to note that the real components of the continuous wavelet transform along the ridge are directly proportional to the signal given by Eq. (2) and from Eq. (42) we obtain

$$A(b) = 2\frac{|W_\psi[x](a(b),b)|}{\sqrt{N\pi}\sqrt{a(b)}}, \tag{43}$$

$$\varphi(b) = \mathrm{Arg}(W_\psi[x](a(b),b)). \tag{44}$$

The ridge and the skeleton of the continuous wavelet transform will be used for the estimation of the instantaneous amplitude $A(t)$ and instantaneous angular frequency $\dot{\varphi}(t)$. From Eqs. (43) and (44) we can compute $\dot{A}(t)$ and $\dot{\beta}(t) = \dot{\varphi}(t) - \omega_n$ that will be used with Eqs. (14) and (23) to identify nonlinearities on damping and stiffness and quantify their values.

Finally, we use the following procedure for the identification and quantification of nonlinearities in vibrating systems. Once the free response of the mechanism has been measured the skeleton of the continuous wavelet transform is extracted to obtain the envelope $A(t)$ and its derivative $\dot{A}(t)$. We form then the equation $\dot{A}(t) = \sum_{i=0}^{p} c_i A^i(t)$. If $p = 1$, we obtain the equation of a straight line and from the slope of this line we estimate c_1 and the damping coefficient from Eq. (15). If $p \neq 1$, a polynomial is obtained. The coefficients c_0, $c_1, \ldots, c_p$ of the polynomial, of a specified degree p, are those that best fit the data in a least-squares sense. Once the coefficients c_0, $c_1, \ldots, c_p$ have been computed the damping coefficients are estimated from Eq. (15). From the skeleton of the wavelet transform we extract also the phase $\varphi(t)$ and its derivative $\dot{\varphi}(t)$, representing the instantaneous angular frequency of the system. Representations of vibration behaviour in the form of curves of free vibration envelope versus instantaneous frequency are called backbone curves. For linear systems a backbone does not depend of the envelope and is constant. For systems with nonlinearities on stiffness the backbone is not constant and following the form of the backbone we obtain a softening system or a hardening system. The backbone is obtained from $\dot{\varphi}(t) = \omega_n + r_q A^{q-1}(t)$ and the natural frequency ω_n is estimated from the backbone for $A(t) = 0$. The degree q of the polynomial and the coefficient r_q are obtained by minimization of the normalized root mean square error (RMSE) between the measured value of the instantaneous angular frequency $\dot{\varphi}(t)$ obtained from the skeleton of the continuous wavelet transform and the identified value $\tilde{\dot{\varphi}}(t)$ of the mechanical model

$$\mathrm{RMSE}(\tilde{\dot{\varphi}}) = \sqrt{\frac{\sum_{i=1}^{T} [\dot{\varphi}(t_i) - \tilde{\dot{\varphi}}(t_i)]^2}{\sum_{i=1}^{T} \dot{\varphi}(t_i)^2}}, \tag{45}$$

where T is the number of samples. The value of the normalized root mean square error is a measure of the accuracy of the fit. Once r_q has been obtained the stiffness coefficient is estimated from Eq. (24). For multi-component signals we use the time–frequency localization properties of the continuous wavelet transform and the property of linearity. It is possible to follow for each ith mode the envelope decay $A_i(t)$, the phase variations $\varphi_i(t)$, their derivatives and estimate nonlinearities.

4. Applications

4.1. Numerical examples

In order to show the usefulness of nonlinearities identification and quantification procedures, simulations were performed. The simulated data was corrupted by zero mean Gaussian noise. The signal-to-noise ratio (SNR) is defined as $\mathrm{SNR} = 10 \log_{10}(\mathrm{var(signal)}/\mathrm{var(noise)})$.

4.1.1. System with viscous damping and cubic stiffness nonlinearities

The first example considered involves a sdof system with viscous damping and cubic stiffness nonlinearities. The equation of motion is of the kind:

$$\ddot{x}(t) + \mu_1 \dot{x}(t) + \omega_n^2 x(t) + \eta_3 x^3(t) = 0, \tag{46}$$

where $\mu_1 = 0.7\ \mathrm{s}^{-1}$; $\omega_n = 20\ \mathrm{rad\ s}^{-1}$; $\eta_3 = 500\ \ (\mathrm{m\,s})^{-2}$. The system was simulated using a fourth-order Runge–Kutta procedure with initial displacement $x(0) = 0.5\,\mathrm{m}$. The number of data samples was 2048 and the time record 12 s. The signal was additionally corrupted by zero mean Gaussian noise with $\mathrm{SNR} = 15\,\mathrm{dB}$.Fig. 1 shows the response of the noisy signal. Fig. 2 shows the continuous wavelet transform amplitude for the noisy signal using the traditionally Morlet wavelet given by Eq. (32). To improve the resolution we choose the modified Morlet wavelet given by Eq. (34) and determine the parameter N by minimization of the wavelet entropy (38). As shown in Fig. 3 the minimal value of N is 13. This value is the optimal value used in the modified Morlet wavelet. Fig. 4 shows the amplitude of the continuous wavelet transform for the noisy signal and its ridge when $N = 13$. From the ridge we extract the skeleton of the continuous wavelet transform. The real part of the skeleton gives the recovered signal. Fig. 5 shows the comparison between the theoretical free response obtained from Eq. (46) in solid line and the identified free response obtained from the skeleton of the continuous wavelet transform in dashed line. These plots are in good agreement apart from the beginning and

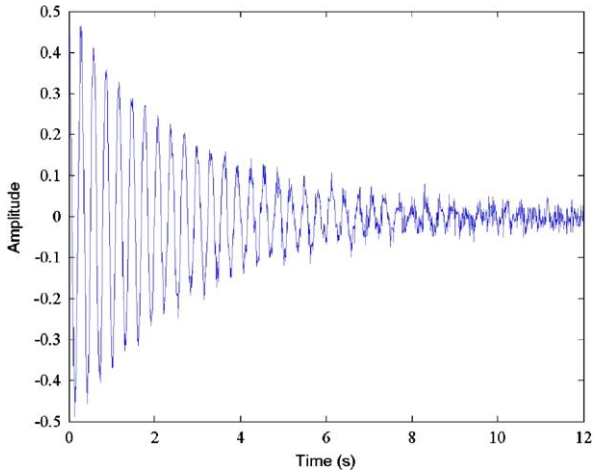

Fig. 1. Free response function for the oscillator with viscous damping and cubic stiffness (SNR = 15 dB).

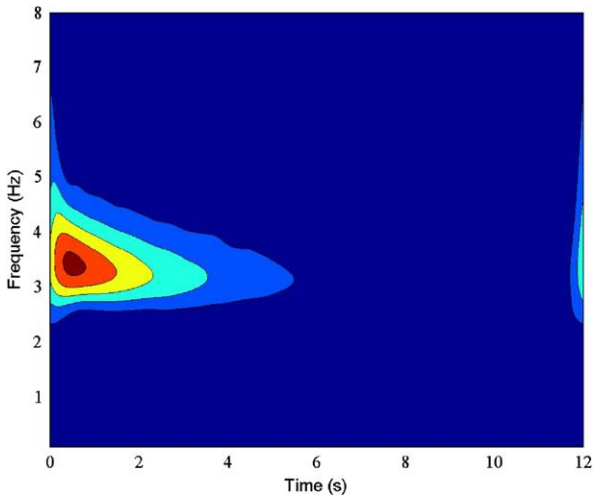

Fig. 2. Continuous wavelet transform amplitude for the noisy signal with $N = 2$.

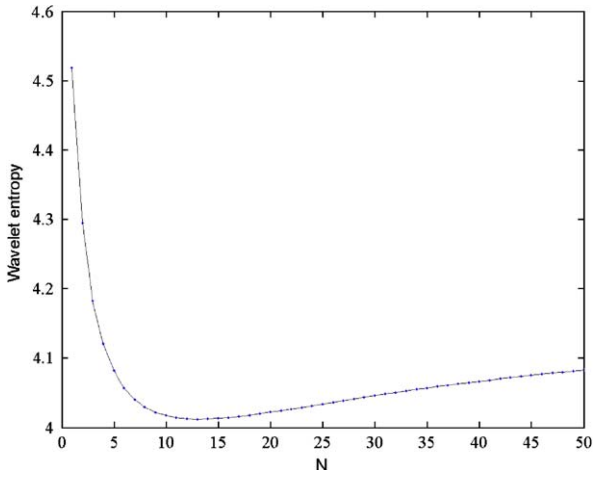

Fig. 3. Variations of the wavelet entropy.

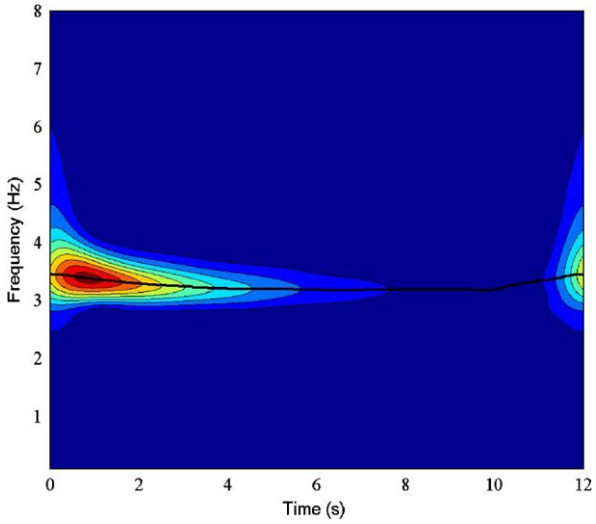

Fig. 4. Continuous wavelet transform amplitude and its ridge for the noisy signal with $N = 13$.

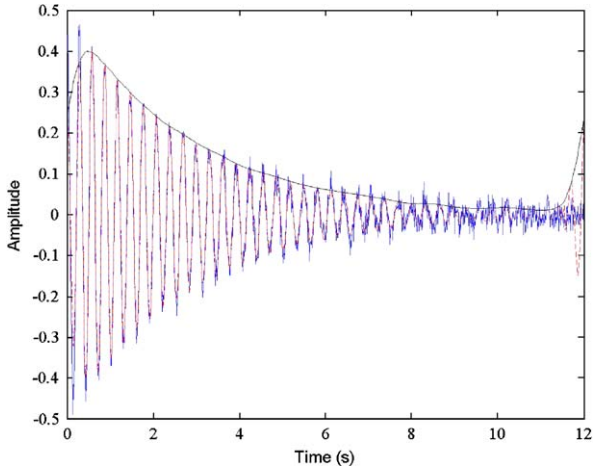

Fig. 5. Theoretical free response (solid line) and recovered free response from the skeleton of the continuous wavelet transform (dashed line) (SNR = 15 dB).

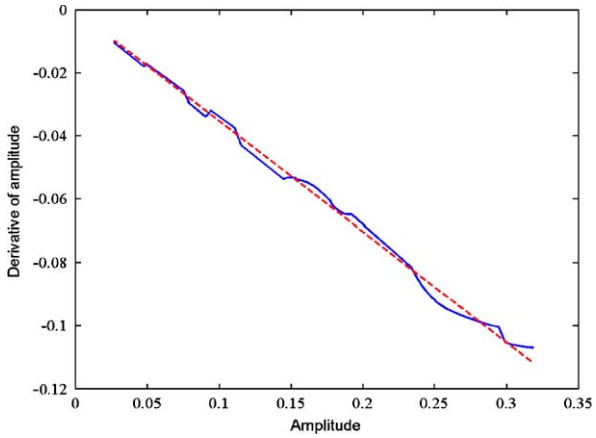

Fig. 6. Variations of $\dot{A}$ as a function of A from the skeleton of the continuous wavelet transform (solid line) and from the identified mechanical system (dashed line).

the end of the data due to edge effect. The problem of edge effect has been studied by Slavic et al. [9], Le and Argoul [23], Kijewski and Kareem [24]. Note that the edge effect can be reduced by adding zeros or by adding negative values of the signal at the beginning and the end of the signal [24]. The modified signal is called "signal padding". The envelope of the identified signal obtained from Eq. (43) is also plotted in Fig. 5. Fig. 6 shows the variations of $\dot{A}$ as a function of A. The characteristics of the analysed system obtained from the skeleton of the continuous wavelet transform given by a solid line, show very good agreement with the identified characteristics given by a dashed line and obtained from the oscillator model. This figure clearly shows the presence of viscous damping in the system since we obtain a straight line. From the slope of this line we estimate the damping coefficient μ_1 since $\dot{A} = c_1 A = -\mu_1 A/2$. Fig. 7 shows the backbone curve of the analysed system (solid line) obtained from the skeleton of the wavelet transform and the backbone curve of the identified system (dashed line). From this plot we obtain the value of f_n for $A = 0$. Table 1 shows the RMSE between measured values of the instantaneous angular frequency $\dot{\varphi}(t)$ obtained from the skeleton of the wavelet transform and identified values $\tilde{\dot{\varphi}}(t_i)$ of the estimated oscillator model for different orders q and values of r_q. It is clear that the optimal value is $q = 3$, we have then a cubic stiffness nonlinearity. From Eqs. (23) and (24) we obtain $\dot{\varphi}(t) = \omega_n + 3\eta_3 A^2(t)/8\omega_n$ and we can compute from this expression the value of η_3. Table 2

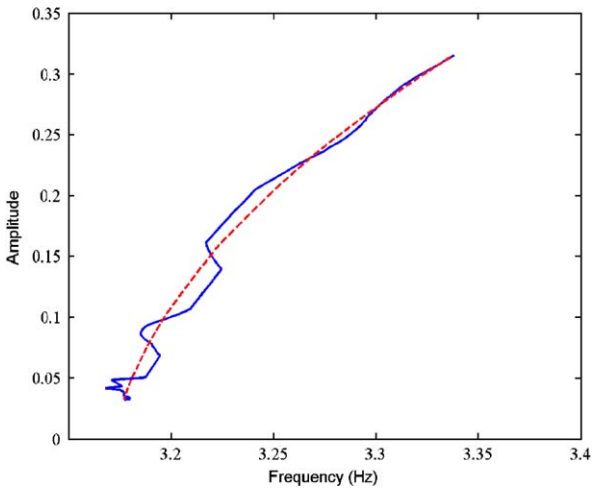

Fig. 7. Backbone curves for the measured (solid line) and identified mechanical system (dashed line).

Table 1
Estimation of the order q for the oscillator with viscous damping and cubic stiffness nonlinearities

q	$q = 1$	$q = 3$	$q = 5$	$q = 7$
$\omega = \omega(A)$	$\omega = \omega_n + \frac{\eta_1}{2\omega_n}$	$\omega = \omega_n + \frac{3}{8}\frac{\eta_3}{\omega_n}A^2$	$\omega = \omega_n + \frac{5}{16}\frac{\eta_5}{\omega_n}A^4$	$\omega = \omega_n + \frac{35}{128}\frac{\eta_7}{\omega_n}A^6$
RMSE($\tilde{\dot{\varphi}}$)	0.0130	1.7291e−004	0.0055	0.0082

Table 2
Parameter identification for the oscillator with viscous damping and cubic stiffness nonlinearities

Parameters	μ_1 (s^{-1})	$\Delta\mu_1$ (%)	ω_n (rad s^{-1})	$\Delta\omega_n$ (%)	η_3 $(m\,s)^{-2}$	$\Delta\eta_3$ (%)
Exact	0.7		20		500	
Identified, SNR = ∞	0.702	0.3	20.005	0.03	502.044	0.41
Identified, SNR = 20 dB	0.702	0.3	20.007	0.04	497.265	−0.55
Identified, SNR = 15 dB	0.690	−1.4	20.018	0.10	495.175	−0.97

shows the system parameter identification and the errors in per cent between exact values and identified values for different levels of Gaussian noise added to the data. Even with important noise satisfactory results are obtained.

4.1.2. System with composite damping and nonlinear stiffness

The second example considered involves a sdof system with composite damping including Coulomb, linear and quadratic damping and a cubic stiffness nonlinearity. The equation of motion is

$$\ddot{x} + \mu_0 \operatorname{sgn}(\dot{x}) + \mu_1 \dot{x} + \mu_2 \dot{x}|\dot{x}| + \omega_n^2 x + \eta_3 x^3 = 0 \tag{47}$$

with $\mu_0 = 0.13\,\mathrm{m\,s^{-2}}$; $\mu_1 = 0.6\,\mathrm{s^{-1}}$; $\mu_2 = 0.1\,\mathrm{m^{-1}}$; $\omega_n = 20\ \mathrm{rad\,s^{-1}}$; $\eta_3 = 500\ (\mathrm{m\,s})^{-2}$. The free response of the system was simulated using a fourth-order Runge–Kutta procedure with initial displacement $x(0) = 0.5\,\mathrm{m}$. The number of data samples was 2048 and the time record 9 s. Fig. 8 shows the amplitude of the continuous wavelet transform and its ridge. From the ridge we extract the skeleton of the continuous wavelet transform. Fig. 9 gives a comparison between real part of the continuous wavelet transform skeleton obtained from the ridges and the theoretical free response. The envelope of the identified signal is also plotted. This, apart the

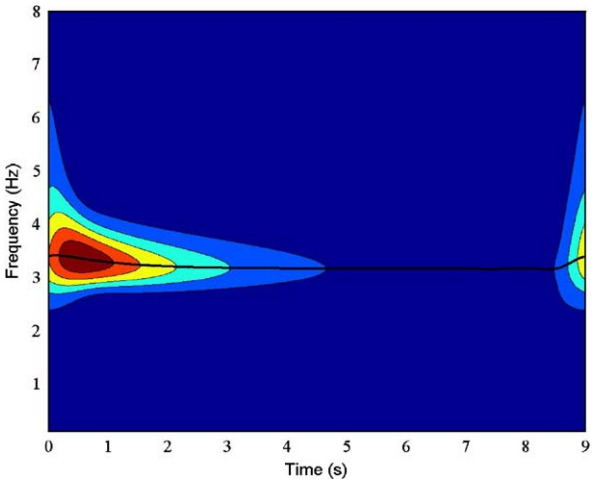

Fig. 8. Continuous wavelet transform amplitude and its ridge for the oscillator with composite damping and nonlinear stiffness.

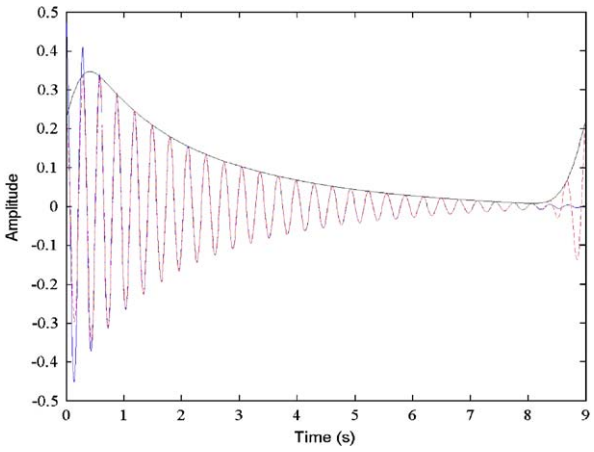

Fig. 9. Theoretical free response (solid line) and recovered free response from the skeleton of the continuous wavelet transform (dashed line).

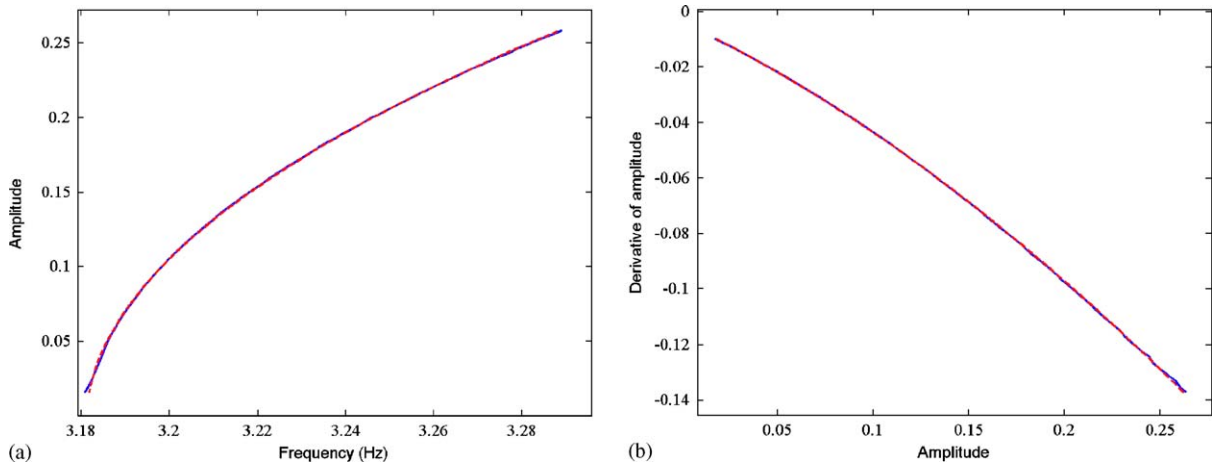

Fig. 10. (a) Backbone curves for the measured (solid line) and identified mechanical system (dashed line); (b) variations of $\dot{A}$ as a function of A for the measured (solid line) and identified mechanical system (dashed line).

Table 3
Parameter identification for the oscillator with composite damping and cubic stiffness nonlinearities

Parameters	μ_0 ($m\,s^{-2}$)	$\Delta\mu_0$ (%)	μ_1 (s^{-1})	$\Delta\mu_1$ (%)	μ_2 (m^{-1})	$\Delta\mu_2$ (%)
Exact	0.13		0.6		0.1	
Identified, SNR $= \infty$	0.1297	−0.2	0.6235	3.9	0.0974	−2.6
Identified, SNR = 20 dB	0.1343	3.3	0.5941	−1	0.1025	2.5
Identified, SNR = 15 dB	0.1217	−6.3	0.6247	4.1	0.0981	−1.9%
Parameters	ω_n ($rad\,s^{-1}$)	$\Delta\omega_n$ (%)	η_3 $(m\,s)^{-2}$	$\Delta\eta_3$ (%)		
Exact	20		500			
Identified, SNR $= \infty$	19.993	−0.035	507.45	1.5		
Identified, SNR = 20 dB	19.982	−0.09	526.01	5.2		
Identified, SNR = 15 dB	19.971	−0.45	545.99	9		

beginning and the end of the data, shows perfect match of signals. Fig. 10 shows the backbone curves and the variations of $\dot{A}$ as a function of A for the measured and identified mechanical system. These results clearly displays the nonlinear characteristics of the system. The natural frequency is estimated from the backbone curve for $A = 0$; the order q and the coefficient of nonlinear stiffness are obtained using the RMSE($\tilde{\varphi}$) procedure described previously. Damping coefficients are estimated from a polynomial interpolation of the continuous parabola obtained in Fig. 10(b). The characteristics obtained from the skeleton of the continuous wavelet transform given by a solid line, show very good agreement with the theoretical characteristics identified from the oscillator model and given by a dashed line. The estimated values of parameters and their errors for different levels of noise are presented in Table 3. The results are again satisfactory.

4.1.3. 2dof system with nonlinear stiffness

A 2dof system with cubic stiffness nonlinearity is considered. Fig. 11 shows the 2dof the system. The differential equations governing the system are

$$\begin{aligned} m_1\ddot{x}_1 + (c_1 + c_2)\dot{x}_1 + (k_1 + k_2)x_1 - k_2x_2 - c_2\dot{x}_2 - k_4x_1^3 = 0, \\ m_2\ddot{x}_2 + (c_2 + c_3)\dot{x}_2 + (k_2 + k_3)x_2 - k_2x_1 - c_2\dot{x}_1 = 0 \end{aligned} \quad (48)$$

with $m_1 = m_2 = 1\,kg$; $c_1 = 0.08\,N\,s\,m^{-1}$; $c_2 = 0.03\,N\,s\,m^{-1}$; $c_3 = 0.05\,N\,s\,m^{-1}$; $k_1 = 3\,N\,m^{-1}$; $k_2 = 10\,N\,m^{-1}$; $k_3 = 5\,N\,m^{-1}$; $k_4 = 170\,N\,m^{-3}$. The eigenfrequencies of the linear system are $f_1 = 0.316\,Hz$ and $f_2 = 0.780\,Hz$.

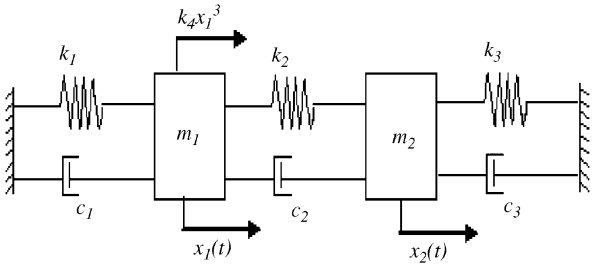

Fig. 11. 2dof system with nonlinearities on stiffness.

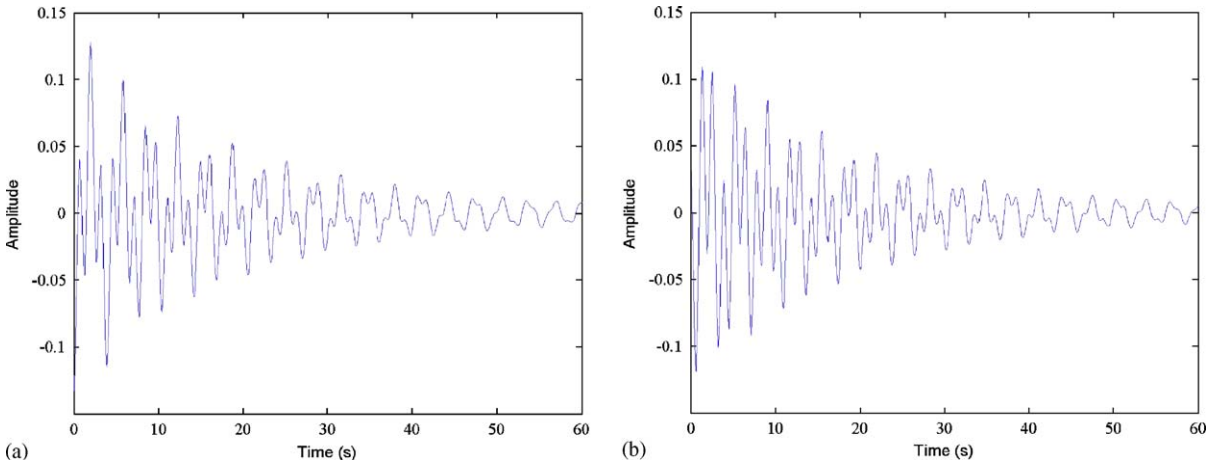

Fig. 12. Free response functions for the 2dof system: (a) $x_1(t)$; (b) $x_2(t)$.

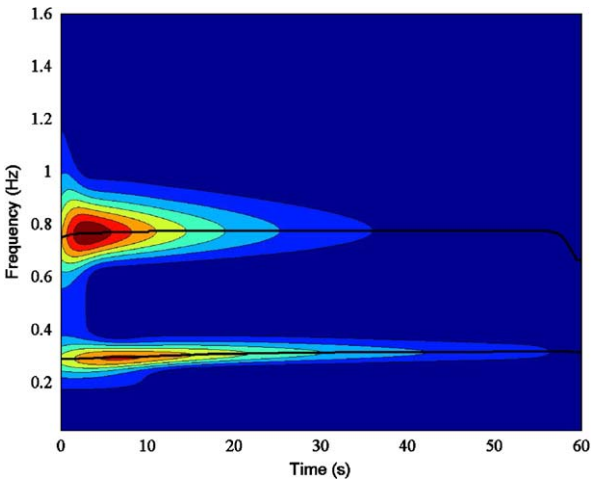

Fig. 13. Continuous wavelet transform amplitude and its ridge for the 2dof system from $x_2(t)$.

The free response of the system was simulated using a fourth-order Runge–Kutta procedure with initial displacements $x_1(0) = -0.14\,\text{m}$ and $x_2(0) = 0.04\,\text{m}$. Fig. 12 shows the free responses $x_1(t)$ and $x_2(t)$ of the system. The continuous wavelet transform is applied to the response $x_2(t)$. Analogous results are obtained if we consider $x_1(t)$. The amplitude of the continuous wavelet transform and the ridge are given in Fig. 13. Two vibration modes can be observed. It has been shown in Section 3 that the continuous wavelet transform is a signal decomposition procedure working as a filter in the time-scale (or time–frequency) domain. It is possible

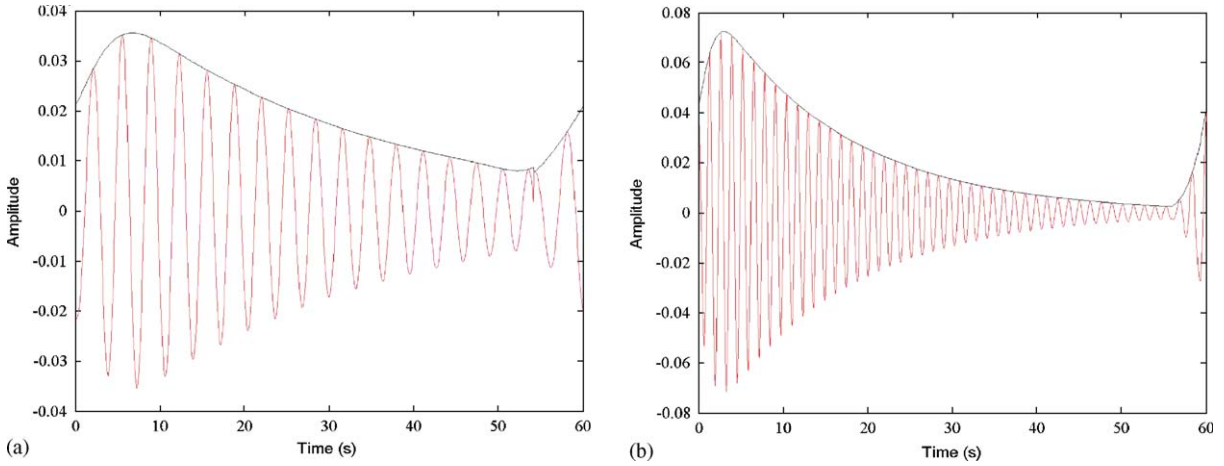

Fig. 14. Measured mode in time domain from the skeleton of the continuous wavelet transform and its envelope: (a) first mode; (b) second mode.

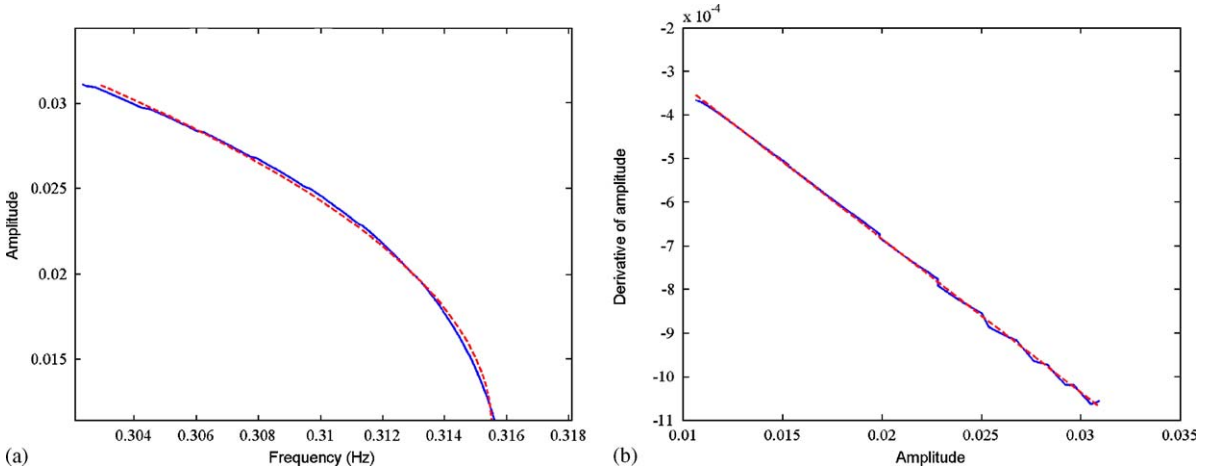

Fig. 15. (a) Backbone curves for the measured (solid line) and identified (dashed line) first mode; (b) variations of $\dot{A}$ as a function of A for the measured (solid line) and identified (dashed line) first mode.

to isolate each mode and to follow the envelope decay and the phase variation in time for each isolated mode. We can then identify and quantify nonlinearities of each mode. The validity of this decoupling procedure is strictly linked with the wavelet frequency resolution, that is with the continuous wavelet transform capability of separating close modes. The ridge detection procedure was applied twice, separately for each mode. Fig. 14 shows the measured modes in time domain obtained from the real part of the skeleton of the continuous wavelet transform. The backbones for these two modes and the variations of derivative of amplitude are also plotted in Figs. 15 and 16. The backbones clearly show a softening system with cubic stiffness nonlinearities which is confirmed by the computation of RMSE($\tilde{\varphi}$): its minimum value is obtained for $q = 3$. Figs. 15(b) and 16(b) show the presence of viscous damping, since we obtain a straight line which pass by the origin. The characteristics obtained from the skeleton of the continuous wavelet transform given by a solid line, show very good agreement with the identified characteristics of the 2dof system given by a dashed line. The estimated values of parameters with the computation of RMSE($\tilde{\varphi}$) for each mode are presented in Tables 4 and 5 where a noise of level SNR = 15 dB has been added to the signal. The results obtained are satisfactory.

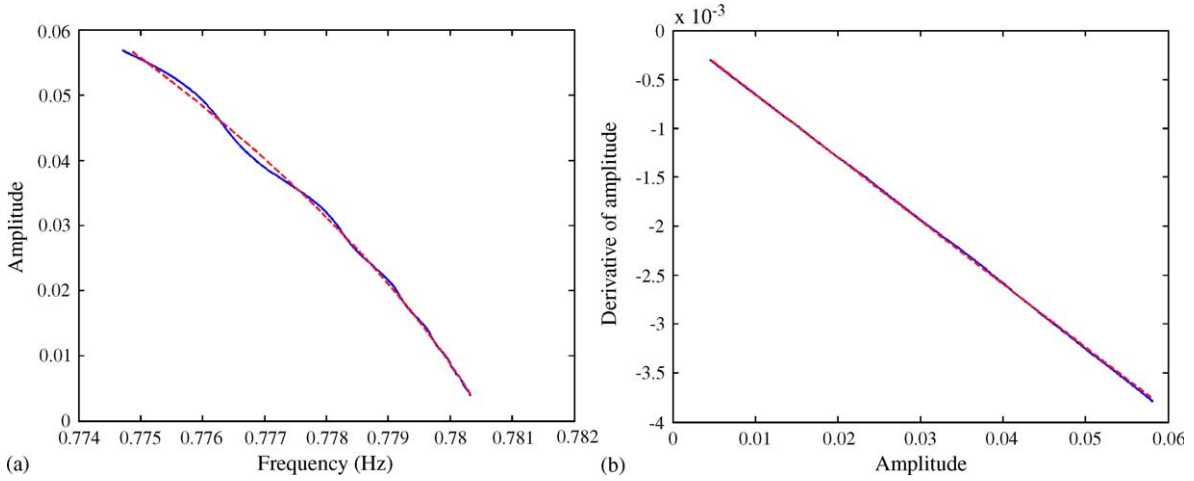

Fig. 16. (a) Backbone curves for the measured (solid line) and identified (dashed line) second mode; (b) variations of $\dot{A}$ as a function of A for the measured (solid line) and identified (dashed line) second mode.

Table 4
Parameter identification for the 2dof system without noise

Mode	f_n (Hz)	μ_1 (s^{-1})	η_3 $(m\,s)^{-2}$	RMSE($\tilde{\hat{\varphi}}$)
1	0.316	0.067	302	5.5×10^{-4}
2	0.780	0.128	157	9×10^{-5}

Table 5
Parameter identification for the noisy 2dof system (SNR = 15 dB)

Mode	f_n (Hz)	μ_1 (s^{-1})	η_3 $(m\,s)^{-2}$	RMSE($\tilde{\hat{\varphi}}$)
1	0.316	0.068	296	14×10^{-4}
2	0.781	0.127	134	25×10^{-4}

4.2. Experimental measurements

4.2.1. Experiment nonlinear system

Experiments were carried out at the Applied Mechanics Laboratory of Besançon. The structure used for the experiment was a mild steel clamped-free beam mounted so that its motion was confined to the horizontal plane as shown in Fig. 17. Nonlinearities on stiffness and damping were created punctually on points 1 and 2 via a negative feedback. A displacement sensor was placed at measurement point 1. The signal obtained was then passed through two multiplier networks to obtain $x^3(t)$. The cubic signal was amplified using a power amplifier, we can then obtain different levels of nonlinearities on stiffness. The signal is passed through an electromagnetic shaker to obtain a negative feedback. A nonlinearity on stiffness of the form $\eta_3 x^3(t)$ is then created.

A velocity sensor was placed at measurement point 2 and the signal obtained was then passed through a rectifier network and a multiplier network to obtain $\dot{x}^2(t)\,\mathrm{sgn}(\dot{x}(t))$. The signal was amplified using a power amplifier, we can then obtain different levels of nonlinearities on damping. This signal was passed through an electromagnetic shaker to obtain a negative feedback. A nonlinearity on damping of the form $\mu_2 \dot{x}^2(t)\,\mathrm{sgn}(\dot{x}(t))$ is then obtained. The beam was excited on point 3 using an electromagnetic exciter. The excitation was stopped and the free response of the system was recorded. The layout of the feedback loop is shown in Fig. 17. Even if the beam is a multi dof system, the study is focused on the identification of a sdof: the first mode of vibration.

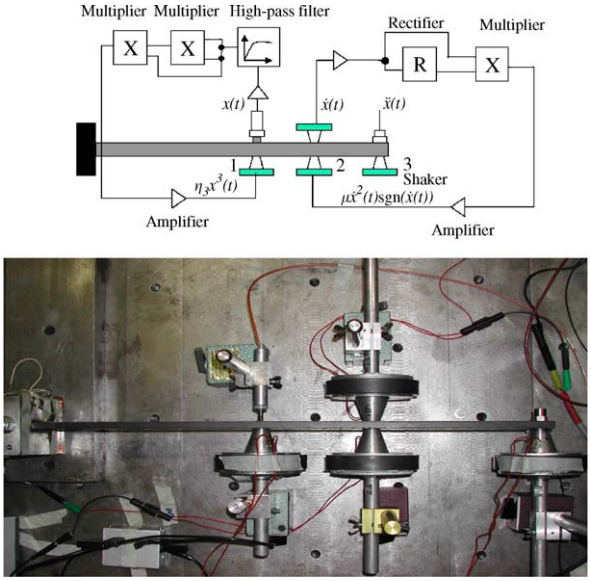

Fig. 17. Feedback loop for the introduction of nonlinearities and experimental system.

4.2.2. Nonlinearities on stiffness

Following the gain obtained from the power amplifier used in the experimental procedure, different values of nonlinearities on stiffness are considered on point 1. In our application three tests have been performed corresponding qualitatively to a weak, a medium and a strong nonlinearity on stiffness. The parameter identification and quantification procedure was performed as previously on the base of decaying envelopes. More precisely we compute the derivative of amplitude $\dot{A}$ as a function of the amplitude A and backbone curves. The analysed vibration data shown in Fig. 18(a) is a free response obtained from the experimental test beam with a medium cubic stiffness nonlinearity, using the sensor displacement on point 1. The excitation was stopped at $t = 0.9$ s and the free response of the beam was considered in the continuous wavelet transform to obtain modal parameters. Fig. 18(b) shows the measured and the recovered free response of the system obtained from the real part of the continuous wavelet transform skeleton. These plots are in good agreement apart from the beginning and the end of the data due to edge effect. The envelope of the recovered signal is also plotted. The natural frequency is estimated from the backbone curve shown in Fig. 18(c). The order q and the coefficient of nonlinear stiffness is obtained by minimization of the root mean square error between the instantaneous frequency measured from the skeleton of the continuous wavelet transform and the instantaneous frequency of the estimated oscillator model. The measured and identified backbones curves are presented in Fig. 18(c) showing very good agreement. Fig. 18(d) shows the variations of $\dot{A}$ as a function of A for the measured and identified signal. This figure clearly shows the viscous damping of the system since we obtain a straight line passing by the origin. The estimated values of parameters for different values of stiffness are presented in Table 6.

The normalized values of RMSE($\tilde{\dot{\varphi}}$) and RMSE($\tilde{\dot{A}}$) are given in Table 6. These values are very small and we can conclude that the identification of nonlinearities on stiffness and their quantification give satisfactory results. We can conclude that the model of a Duffing oscillator with weak viscous damping gives a good fit for the first mode of this experimental beam. Note, however, that the damping in clamped beam is in general hysteretic and not viscous. Here an equivalent viscous damping has been identified.

4.2.3. Nonlinearities on stiffness and composite damping

Nonlinearities on stiffness are always considered on point 1 and nonlinearities on damping are added on point 2. The parameter identification and quantification procedure was performed as previously on the basis of the measured backbone curve and the decaying envelope from which we obtain the variations of $\dot{A}$ as a

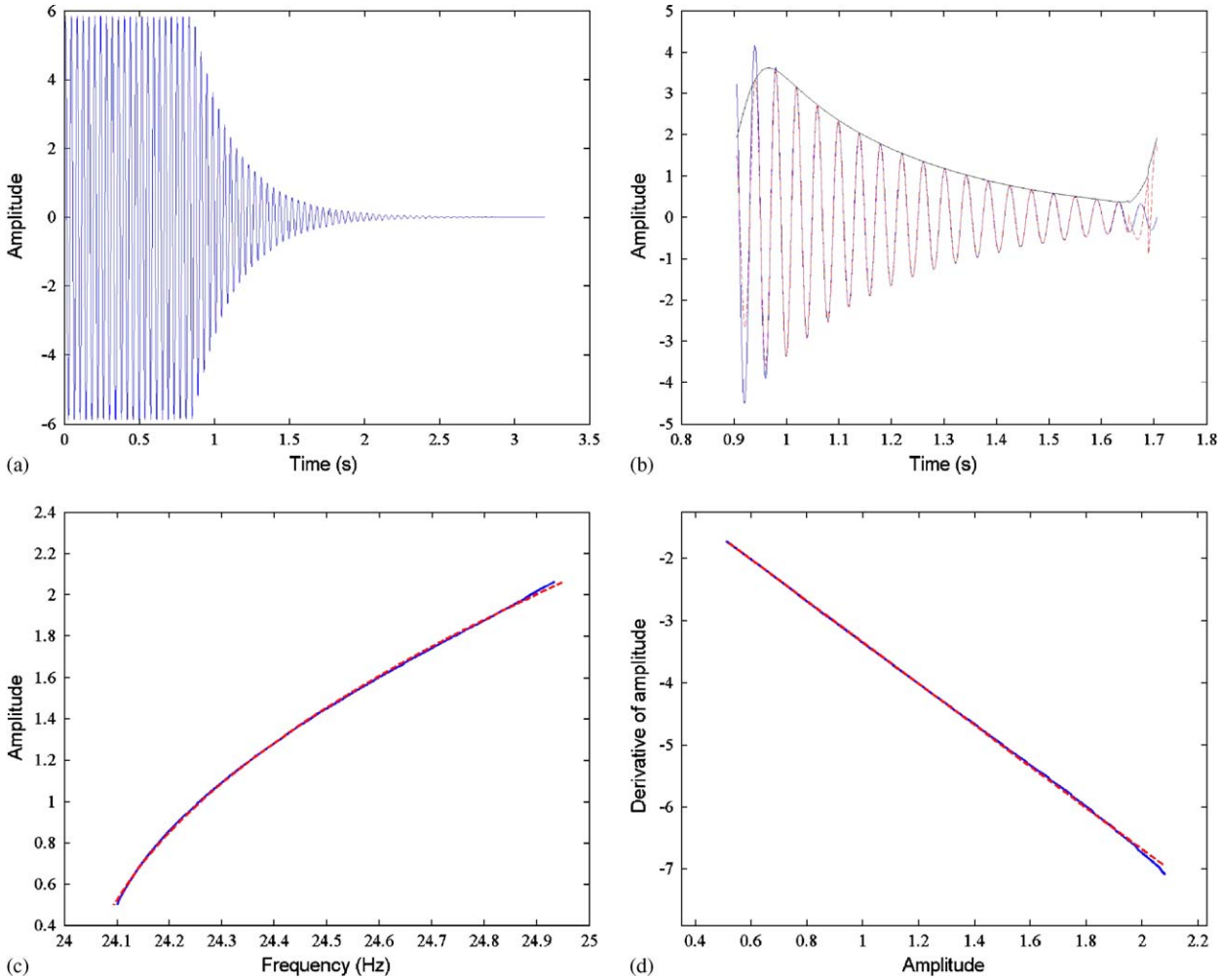

Fig. 18. (a) Measured signal from the displacement sensor on point 1; (b) measured free response (solid line) and identified free response from the skeleton of the continuous wavelet transform (dashed line); (c) backbone curves for the measured (solid line) and identified system (dashed line); (d) variations of $\dot{A}$ as a function of A for the measured (solid line) and identified system (dashed line).

Table 6
Identified results for the beam with nonlinearities on stiffness

Tests	Parameters				
	μ_1 (s^{-1})	f_n (Hz)	η_3 $(m\,s)^{-2}$	RMSE($\tilde{\varphi}$)	RMSE($\tilde{\dot{A}}$)
Weak stiffness	7.073	24.10	224.813	1.953e−004	0.0035
Medium stiffness	6.962	24.08	490.553	1.869e−004	0.0065
Strong stiffness	6.999	23.97	1148.7	4.660e−005	0.0012

function of A. Fig. 19(a) shows the measured time response obtained from the displacement sensor on point 1 and the recovered time response obtained from the skeleton of the continuous wavelet transform. These plots show perfect match of both signals. From the measured signal we plot the amplitude of the wavelet transform

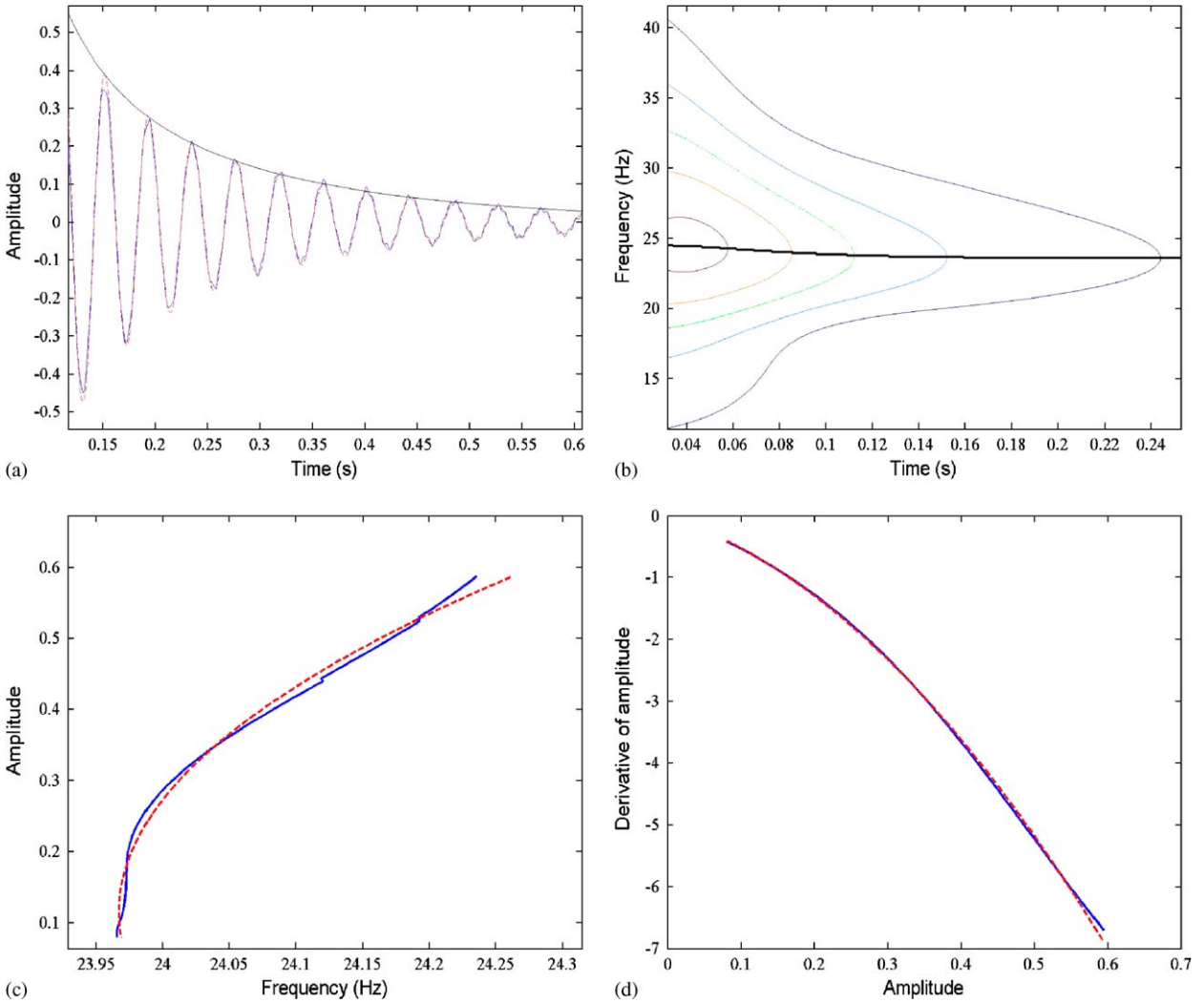

Fig. 19. (a) Measured free response (solid line) and recovered free response from the skeleton of the continuous wavelet transform (dashed line); (b) wavelet transform amplitude and ridge; (c) backbone curves for the measured (solid line) and identified system (dashed line); (d) variations of $\dot{A}$ as a function of A for the measured (solid line) and identified system (dashed line).

Table 7
Identified results for the beam with nonlinearities on stiffness and damping

	Parameters					
	μ_1 (s^{-1})	μ_2 (m^{-1})	f_n (Hz)	η_3 $(m\,s)^{-2}$	RMSE($\tilde{\varphi}$)	RMSE($\tilde{\dot{A}}$)
Identified	7.214	0.205	23.98	1135	2.02e−004	0.0026

and its ridge in Fig. 19(b). Finally, Figs. 19(c) and (d) show backbone curves and measured and identified plots of $\dot{A}$ as a function of A. The estimated values of parameters are presented in Table 7 with the computation of the normalized root mean square errors: RMSE($\tilde{\varphi}$) and RMSE($\tilde{\dot{A}}$).

The small values of RMSE($\tilde{\hat{\varphi}}$) and RMSE($\tilde{\hat{A}}$) confirms that the identification has provided good results. We can conclude that the model of a Duffing oscillator with weak viscous and quadratic damping describes correctly the first mode of this experimental beam.

5. Conclusion

A time-scale analysis is used for identification, classification and quantification of weak nonlinearities on damping and stiffness in vibrating systems. The proposed approach cannot be applied for all kinds of nonlinear dynamical systems, in a "blind way", but for oscillators with weak nonlinearities on damping and stiffness. The procedure is based on the ridges and skeletons of the continuous wavelet transform. While a great number of authors use the Morlet wavelet function as analysing function, the modified Morlet wavelet function has been used in this paper. Its time and frequency resolution can be altered by adjusting the value of a parameter N. The optimal value of N has been obtained by minimization of the wavelet entropy. The effectiveness of the proposed method has been demonstrated using numerical results for a sdof and 2dof system with nonlinearities on damping and stiffness. The procedure was also tested experimentally on a clamped beam where nonlinearities on damping and stiffness have been added. These experimental results validate the procedure of identification and quantification of weak nonlinearities on damping and stiffness based on the ridges and skeletons of the continuous wavelet transform. The procedure is applied to free responses of vibrating systems and has the advantage of not requiring knowledge of the excitation forces. However, some effort should be spent for the extension of the technique to the analysis of industrial systems with nonlinearities. The continuous wavelet transform technique has the advantage that it requires to measure only displacements or velocities or accelerations of the system. It is not necessary to measure displacements and velocities and accelerations simultaneously as in the case of non-parametric methods.

References

[1] M. Feldman, Non-linear free vibration identification via the Hilbert transform, *Journal of Sound and Vibration* 208 (1997) 475–489.
[2] S.F. Masri, T.K. Caughey, A nonparametric identification technique for nonlinear dynamic problems, *Journal of Applied Mechanics* 46 (1979) 433–447.
[3] R.J. Shyu, A spectral method for identifying nonlinear structures, *Modal Analysis* 9 (1994) 255–268.
[4] C.B. Yun, M. Shinozuka, Identification of nonlinear structural dynamic systems, *Journal of Structural Mechanics* 8 (1980) 187–203.
[5] J.N. Yang, S. Lin, On-line identification of non-linear hysteretic structures using an adaptive tracking technique, *International Journal of Non-linear Mechanics* 39 (2004) 1481–1491.
[6] M. Ruzzene, A. Fasana, L. Garibaldi, B. Piombo, Natural frequencies and damping identification using the wavelet transform: application to real data, *Mechanical Systems and Signal Processing* 11 (1997) 207–218.
[7] S.A. Neild, P.D. McFadden, M.S. Williams, A review of time–frequency methods for structural vibration analysis, *Engineering Structures* 25 (2003) 713–728.
[8] W.J. Staszewski, Identification of damping in MDOF systems using time-scale decomposition, *Journal of Sound and Vibration* 203 (1997) 283–305.
[9] J. Slavic, I. Simonovski, M. Boltezar, Damping identification using a continuous wavelet transform: application to real data, *Journal of Sound and Vibration* 262 (2003) 291–307.
[10] J. Lardies, S. Gouttebroze, Identification of modal parameters using the wavelet transform, *International Journal of Mechanical Sciences* 44 (2002) 2263–2283.
[11] W.J. Staszewski, Identification of non-linear systems using multi-scale ridges and skeletons of the wavelet transform, *Journal of Sound and Vibration* 214 (1998) 639–658.
[12] P. Argoul, T.P. Le, Instantaneous indicators of structural behaviour based on the continuous Cauchy wavelet analysis, *Mechanical Systems and Signal Processing* 17 (2003) 243–250.
[13] L. Garibaldi, M. Ruzzene, A. Fasana, B. Piombo, Identification of nonlinear damping mechanisms using the wavelet transform, *Mécanique Industrielle et Matériaux* 51 (1998) 92–94.
[14] V. Lenaerts, G. Kerschen, J.C. Golinval, M. Ruzzene, E. Giorcelli, Validation of two nonlinear system identification techniques using experimental testbed, *Shock and Vibration* 11 (2004) 365–375.
[15] C.M. Harris, *Shock and Vibration Handbook*, McGraw-Hill, New York, 1995.
[16] A.H. Nayfeh, *Perturbation Methods*, Wiley, New York, 1973.
[17] N. Bogolioubov, I. Mitropolski, *Les méthodes Asymptotiques en Théorie des Oscillations nonlinéaires*, Gauthier-Villars édition, 1962.
[18] S. Mallat, *Une exploration des Signaux en Ondelettes*, Editions de l'Ecole Polytechnique, 2000.
[19] C.K. Chui, *An Introduction to Wavelets*, Academic Press, New York, 1992.

[20] B. Torresani, *Analyse Continue par Ondelettes*, CNRS Editions, Paris, 1995.
[21] A. Spataru, *Fondements de la théorie de la transmission et du signal*, Presses Polytechniques Romandes, Lausanne, 1987.
[22] J. Lin, L. Qu, Feature extraction based on Morlet wavelet and its application for mechanical fault diagnosis, *Journal of Sound and Vibration* 234 (2000) 135–148.
[23] T.P. Le, P. Argoul, Continuous wavelet transform for modal identification using free decay response, *Journal of Sound and Vibration* 277 (2004) 73–100.
[24] T. Kijewski, A. Kareem, On the presence of end effects and their melioration in wavelet-based analysis, *Journal of Sound and Vibration* 256 (2002) 980–988.